PERGAMON

International Journal of Heat and Mass Transfer 41 (1998) 2947–2959

International Journal of HEAT and MASS TRANSFER

A zero-dimensional model for spray droplet vaporization at high pressures and temperatures

T. B. Gradinger,* K. Boulouchos

Institut für Energietechnik LVV, Swiss Federal Institute of Technology, 8092 Zürich, Switzerland

Received 22 July 1997; in final form 15 December 1997

Abstract

A zero-dimensional droplet vaporization model for spray simulations is presented along with a numerical solution algorithm. The model is equipped with high-pressure property estimation methods (PEM), taking into account the influence of high pressure on physical properties of liquid and gas and on vapor–liquid equilibrium; as well as with low-pressure PEM, simplified for low pressure. It is shown that good results can be obtained with the model for situations where droplet-internal transport is important and even for heating to the critical state. Differences of results obtained with low- and high-pressure PEM are discussed for vaporization at elevated pressure. © 1998 Published by Elsevier Science Ltd. All rights reserved.

Nomenclature

A_s droplet surface area
B_H heat transfer number
B'_H corrected heat transfer number
B_M mass transfer number
c_p specific heat at constant pressure
C_D drag coefficient
C_p molar heat at constant pressure
D species diffusivity
f fugacity
F number of fuel species
Fo Fourier number
g gravitational acceleration
H molar enthalpy
k heat conductivity
L latent heat of vaporization (specific or molar)
m droplet mass
$\dot{m}$ mass flow rate ($\dot{m} > 0$ if vaporizing)
N total number of species
Nu Nusselt number
p pressure
Pr Prandtl number
$\dot{Q}_g$ rate of heat conduction to the droplet surface
$\dot{Q}_l$ rate of heat conduction to the droplet interior
$\dot{Q}_r$ net rate of radiation to the droplet surface
r radial coordinate
R droplet radius; universal gas constant
Re Reynolds number
Sc Schmitt number
Sh Sherwood number
t time
T temperature
$\mathbf{v}$ velocity
V molar volume
X mole fraction
Y mass fraction
overline mass average in droplet.

Greek symbols

α thermal diffusivity
μ chemical potential; dynamic viscosity
ρ density.

Subscripts

f film average
g gas
i species index
l liquid
r reduced
s surface
0 no forced convection
∞ in homogeneous environment.

* Corresponding author.

0017–9310/98 $19.00 © 1998 Published by Elsevier Science Ltd. All rights reserved
PII: S0017-9310(98)00021-0

Abbreviations
CC critical curve
EOS equation of state
GT gas turbine
PEM property estimation methods
QS quasi steady
VLE vapor–liquid equilbriuim.

1. Introduction

For the numerical simulation of vaporizing sprays, models are needed for a single vaporizing droplet. In this article we look at the idealized case of a single spherical droplet in a homogeneous ambience and exposed to parallel flow. Solutions of this problem may also be used for a droplet vaporizing in a turbulent environment, which is the situation generally encountered in practice. In this case, the state of the 'homogeneous environment' surrounding the droplet is taken as the sum of the mean gas flow variables and appropriately chosen gas turbulence fluctuations (see Shirolkar et al. [1] for a recent review of this subject).

While our current interest is in fuel sprays encountered in gas turbines and diesel engines, the model we discuss is relevant for any vaporizing spray. A key property required for a single-droplet vaporization model for spray simulation is that it must be computationally cheap. The fact that thousands of droplets need to be tracked in a realistic spray simulation puts severe limitations on both memory and CPU time available for the integration of an individual droplet. Nevertheless a number of physical phenomena need to be captured: the influence of forced convection and surface blowing on heat and mass transfer, droplet heatup, droplet-internal motion, or spatially varying properties in liquid and gas phase have all been found to be important. Since fuels used in practice consist of many components with different volatilities and different ignition behavior, multicomponent models need to be used. Furthermore, in internal combustion engines and gas turbines pressures are high, making the assumption of an ideal-gas mixture around the droplet invalid and forcing one to use real-gas equations.

Single vaporizing droplets have been subject to extensive numerical investigation, and different authors have proposed a variety of different models. It is possible to classify these models into two groups: (i) extended models that have been developed to study the physics of a single vaporizing droplet, to derive simplified correlations, or to validate simpler models; (ii) models that have been developed for use in whole-spray simulation. Other classifications of models can be made according to spatial resolution; according to whether the droplet is assumed to be composed of multiple components or of a single component; and according to whether property estimation methods (PEM) are generalized to include high-pressure effects. Here, the term properties is used to denote thermodynamic equations of state, vapor–liquid equilibrium (VLE) conditions, and molecular transport coefficients. If the PEM are valid at low and high pressures, they will be called 'high-p PEM'; if they have been simplified for low pressure, they will be called 'low-p PEM'.

Table 1 summarizes different existing droplet vaporization models. The upper half of the table shows models that have been used to study the physics of droplet vaporization and that are computationally too expensive for use in spray simulations. Matlosz et al., Hsieh et al., Curtis and Farrell, Stengele et al., and Jia and Gogos all focused on the vaporization of a stagnant droplet in a high-pressure environment. The absence of forced convection makes the problem spherically symmetric and thus simple enough for a rigorous formulation of transport equations including high-pressure effects on liquid and gas properties. Stengele et al. discussed the influence of different ambient conditions on bicomponent droplet vaporization for pressures up to 40 bar. For pressures up to 59 atm, Curtis and Farrell systematically studied the influence of various simplifying assumptions to their extended model, while Hsieh et al. investigated high-pressure and near-critical phenomena for single-, two- and three-component droplets and pressures up to 65 atm. Jia and Gogos discussed the influence of different phase-equilibrium formulations for pressures up to 100 atm. A two-dimensional model assuming axially symmetric flow was used by Megaridis and Sirignano to investigate convective effects in the gas phase as well as inside the droplet.

As the lower part of Table 1 shows, for spray simulations a variety of models have been proposed that resolve the droplet in radial direction to capture transient phenomena while treating the gas phase as quasi steady. Resolving the droplet with a minimum of 10 [2] or 20 [3] points, however, severely adds to the storage requirements, especially if one is dealing with multicomponent droplets. Therefore, a model which is zero-dimensional as the one proposed by Renksizbulut et al. is very attractive. We decided to use such a model because in our opinion its accuracy is sufficient, particularly in view of the uncertainties involved in modeling other key subprocesses in sprays like droplet breakup, gas-phase turbulence and droplet-turbulence interaction. Extending Renksizbulut et al.'s [4] work, we use low-p and high-p PEM, discuss differences and evaluate the model's performance at high pressures.

2. Model

In zero-dimensional models, only global droplet quantities such as droplet total mass, average temperature,

Table 1
Different single-droplet vaporization models. The flow field is treated spherically symmetric if resolution = 1 and axially symmetric if resolution = 2

Authors/model	Spatial resolution (dimensions)		PEM	Components	Forced convection	Purpose
	Liquid	Gas				
Matlosz et al. [5]	0	1	high-p	1	No	Study high-pressure droplet vaporization
Curtis and Farrell [6]	1	1	high-p	1	No	
Hsieh et al. [7]	1	1	high-p	Multi	No	
Stengele et al. [8]	1	1	high-p	2	No	
Jia and Gogos [9]	1	1	high-p	Multi	No	
Megaridis and Sirignano [10]	2	2	low-p	2	Yes	Study convection
Abramzon and Sirignano [3]	1	0	low-p	1	Yes	Use in whole-spray simulation
Varnavas and Assanis [11]	1	0	high-p	1	Yes	
Jin and Borman [12]	1	0	high-p	Multi	Yes	
Ayoub and Reitz [2]	1	0	high-p	Multi	Yes	
Renksizbulut et al. [4]	0	0	low-p	Multi	Yes	
Present model	0	0	high-p	Multi	Yes	
'Classical' d^2-law	0	0	low-p	1	No	

average composition and velocity are stored and integrated in time. The problem is one of heat and mass transfer with an interface, with transport occurring between ambience and droplet surface, and between droplet surface and droplet core, respectively. Rates of transport are expressed using simple correlations, as will be seen below.

2.1. Differential equations

We give here the conservation equations governing the temporal evolution of global droplet quantities. Let N be the number of components in the system, including those of the ambient gas. With the vaporization rate $\dot{m}$ defined to be positive when the droplet looses mass, conservation of total droplet mass reads

$$\frac{\mathrm{d}m}{\mathrm{d}t} = -\dot{m} \tag{1}$$

and the species conservation equations read

$$\frac{\mathrm{d}m_i}{\mathrm{d}t} = -\dot{m}_i, \quad i = 1,\ldots,N-1. \tag{2}$$

If we make the simplifying assumption that changes in liquid enthalpy due to changes in liquid composition are negligible, conservation of energy for the droplet becomes

$$\frac{\mathrm{d}\bar{T}_\mathrm{l}}{\mathrm{d}t} = \frac{1}{m}\left(\frac{\dot{Q}_\mathrm{l}}{\bar{c}_\mathrm{pl}} - \dot{m}(T_\mathrm{s} - \bar{T}_\mathrm{l})\right) \tag{3}$$

where the bar denotes mass-averaged liquid quantities and $\dot{Q}_\mathrm{l}$ is the rate of heat conduction into the droplet at the surface.

For conservation of momentum, we consider aerodynamic drag and gravitational forces, so that

$$\frac{\mathrm{d}\mathbf{v}}{\mathrm{d}t} = \frac{1}{m}\left(\frac{\rho_\mathrm{g}(\mathbf{v}_\infty - \mathbf{v})|\mathbf{v}_\infty - \mathbf{v}|}{2}\pi R^2 C_\mathrm{D} + \boldsymbol{g}\frac{4\pi}{3}R^3(\bar{\rho}_\mathrm{l} - \rho_\infty)\right) \tag{4}$$

where $\mathbf{v}$ and $\mathbf{v}_\infty$ are droplet and ambient-gas velocities relative to an inertial frame. For the drag coefficient C_D we use the expression

$$C_\mathrm{D} = \frac{24}{Re_m}(1 + 0.2Re_m^{0.63})(1 + B'_\mathrm{H})^{-0.2}$$

with Re_m and B'_H defined as in Section 2.2.1. This correlation accounts for the influence of Stefan flow on drag and has been shown to be in good agreement with 2-D simulations [13].

2.2. Equations for the flow rates

Generally, the rates of heat conduction to the droplet in liquid and gas at the surface are expressed as

$$\dot{Q}_\mathrm{l} = A_\mathrm{s} Nu_\mathrm{l} k_\mathrm{l} \frac{T_\mathrm{s} - \bar{T}_\mathrm{l}}{2R} \tag{5}$$

$$\dot{Q}_\mathrm{g} = A_\mathrm{s} Nu_\mathrm{g} k_\mathrm{g} \frac{T_\infty - T_\mathrm{s}}{2R}. \tag{6}$$

Likewise, the rates of mass flow of species i away from

the droplet in liquid and gas phase at the surface are expressed as

$$\dot{m}_{\mathrm{l}i} = \dot{m} Y_{\mathrm{l}si} + A_{\mathrm{s}}\, Sh_{\mathrm{l}i}\, \rho_{\mathrm{l}} D_{\mathrm{l}i} \frac{Y_{\mathrm{l}si} - \bar{Y}_{\mathrm{l}i}}{2R} \tag{7}$$

$$\dot{m}_{\mathrm{g}i} = \dot{m} Y_{\mathrm{g}si} + A_{\mathrm{s}}\, Sh_{\mathrm{g}i}\, \rho_{\mathrm{g}} D_{\mathrm{g}i} \frac{Y_{\mathrm{g}si} - Y_{\infty i}}{2R}. \tag{8}$$

Note that in equations (5) and (7) the average liquid state is used instead of the state at the liquid core, since the latter is not known.

Above heat and species flow rates are constrained by the interface conditions

$$\dot{m}_{\mathrm{l}i} = \dot{m}_{\mathrm{g}i} (\equiv \dot{m}_i) \tag{9}$$

and

$$\dot{Q}_{\mathrm{g}} + \dot{Q}_{\mathrm{r}} - \dot{Q}_{\mathrm{l}} = \dot{m} L \tag{10}$$

where $\dot{Q}_{\mathrm{r}}$ is the rate of net radiation to the droplet surface and L is a mass-flow-rate-averaged latent heat, obtained from the partial specific latent heats L_i of species i in mixture as

$$L = \sum_{i=1}^{N} \frac{\dot{m}_i}{\dot{m}} L_i.$$

2.2.1. Expressions for gas-phase Nusselt and Sherwood numbers

In the presence of at least a moderate forced convection, or at low pressures, the heat and mass transfer in the gas-phase boundary layer can be assumed to be in quasi-steady (QS) state [3], in which case Nu_{g} and Sh_{g} can be correlated with Re, Pr and Sc numbers. Different expression for Nu_{g} and Sh_{g} have been proposed and are discussed below.

Spherically Symmetric Analysis. In the absence of forced or natural convection, the gas-phase flow field becomes spherically symmetric. If one assumes the gas phase to be in QS state, enthalpy diffusion to be negligible (to obtain symmetry between heat and mass transfer) and thermal conductivity k, the product of density and diffusivity (ρD) and the specific heat c_ρ to be constant over the radius r, one can analytically integrate the governing equations. If we let v be the mass-average velocity, conservation of energy and species read

$$r^2 \rho v c_{\mathrm{p}} \frac{\mathrm{d}T}{\mathrm{d}r} = \frac{\mathrm{d}}{\mathrm{d}r}\left(r^2 k \frac{\mathrm{d}T}{\mathrm{d}r}\right)$$

and

$$r^2 \rho v c_{\mathrm{p}} \frac{\mathrm{d}Y_i}{\mathrm{d}r} = \frac{\mathrm{d}}{\mathrm{d}r}\left(r^2 \rho D \frac{\mathrm{d}Y}{\mathrm{d}r}\right) \quad i = 1, \ldots, F$$

respectively, where F is the number of fuel species in the system. If we assume that the ambient species (with index $i = F+1, \ldots, N$) are insoluble in the droplet, we get for the Sherwood number (index '0' denotes no forced convection)

$$Sh_{\mathrm{g0}} = 2\frac{\ln(1+B_{\mathrm{M}})}{B_{\mathrm{M}}} \quad \text{where} \quad B_{\mathrm{M}} = \frac{\Sigma_{i=1}^{F}(Y_{si} - Y_{\infty i})}{1 - \Sigma_{i=1}^{F} Y_{si}}.$$

Using condition (10) at the surface, we get for the Nusselt number

$$Nu_{\mathrm{g0}} = 2\frac{\ln(1+B'_{\mathrm{H}})}{B'_{\mathrm{H}}}$$

where

$$B'_{\mathrm{H}} = B_{\mathrm{H}}\left(1 - \frac{\dot{Q}_{\mathrm{r}} + \dot{Q}_{\mathrm{l}}}{\dot{Q}_{\mathrm{g}}}\right) \quad \text{and} \quad B_{\mathrm{H}} = \frac{c_{\mathrm{p}}(T_\infty - T_{\mathrm{s}})}{L}.$$

B_{H} and B_{M} are heat and mass transfer numbers, respectively, and B'_{H} is a heat transfer number corrected for the effect of radiation and droplet heating.

The classical d^2-law (see e.g. Kuo [14]) is obtained from the above equations for the special case of only one fuel species ($F = 1$), no droplet heating, no radiation and unity Lewis number (so that $B_{\mathrm{M}} = B_{\mathrm{H}} \equiv B$ = Spalding's transfer number).

Ranz–Marshall Correlations. Frequently used corrections of Nu_{g} and Sh_{g} for forced convection are those proposed by Ranz and Marshall [15]. They conducted experiments of vaporizing single-component droplets at atmospheric pressure and moderate ambient temperatures for which the factor $\ln(1+B)/B$ was close to one. The proposed forms for Nu_{g} and Sh_{g} are (the prime denotes the limiting case of low transfer rates)

$$Nu'_{\mathrm{g}} = 2 + 0.6 Re^{1/2} Pr^{1/3}$$

and

$$Sh'_{\mathrm{g}} = 2 + 0.6 Re^{1/2} Sc^{1/3}$$

where the factor 0.6 was obtained from comparison to experiment.

The corrections for forced convection and high transfer rates have often been combined heuristically in a multiplicative way:

$$Nu_{\mathrm{g}} = Nu'_{\mathrm{g}}\, Nu_{\mathrm{g0}} = (2 + 0.6\, Re^{1/2} Pr^{1/3}) \frac{\ln(1+B'_{\mathrm{H}})}{B'_{\mathrm{H}}} \tag{11}$$

$$Sh_{\mathrm{g}} = Sh'_{\mathrm{g}}\, Sh_{\mathrm{g0}} = (2 + 0.6\, Re^{1/2} Sc^{1/3}) \frac{\ln(1+B_{\mathrm{M}})}{B_{\mathrm{M}}}. \tag{12}$$

Film Theory (Abramzon and Sirignano). Abramzon and Sirignano [3] used film theory [16] to derive expressions for Nu_{g} and Sh_{g}. As a model problem, they considered the laminar flow around a vaporizing wedge to derive corrections to the film thicknesses due to surface blowing. They obtained

$$Nu_{\mathrm{g}} = 2\frac{\ln(1+B'_{\mathrm{H}})}{B'_{\mathrm{H}}} + (Nu'_{\mathrm{g}} - 2)(1+B'_{\mathrm{H}})^{-0.7}$$

$$Sh_{\mathrm{g}} = 2\frac{\ln(1+B_{\mathrm{M}})}{B_{\mathrm{M}}} + (Sh'_{\mathrm{g}} - 2)(1+B_{\mathrm{M}})^{-0.7}$$

where Nu'_g and Sh'_g are again for the limiting case of low transfer rates.

Renksizbulut et al. Correlations. Renksizbulut et al. [17, 18] proposed correlations similar in form to those derived by Abramzon and Sirignano

$$Nu_g = (2+0.57Re_m^{1/2}\,Pr_f^{1/3})(1+B'_H)^{-0.7}$$

$$Sh_{gi} = (2+0.87Re_m^{1/2}\,Sc_{fi}^{1/3})(1+B_M)^{-0.7}$$

where $Re_m = 2R\rho_\infty v_\infty/\mu_f$ is a 'mixed' Reynolds number, and index f denotes film-averaged values using a '1/2-rule', i.e.

$$T_f = T_s + \tfrac{1}{2}(T_\infty - T_s)$$

$$Y_{fi} = Y_{si} + \tfrac{1}{2}(Y_{\infty i} - Y_{si}).$$

ρ_g, D_{gi}, k_g and c_{pg} are all evaluated at the film state. These correlations have been developed by comparison to experimental data [17] and by comparison to results from 2-D axisymmetrical simulations [18].

2.2.2. Expressions for liquid Nusselt and Sherwood numbers

The transport of heat and mass in the liquid is of a rather transient nature, which is the reason why many authors proposed models, which are one-dimensional in the liquid, while zero-dimensional in the gas phase.

Since, with a zero-dimensional model, there is no possibility to spatially resolve any transients, the only thing one can do is to assume a specific type of transient and, based on this, develop correlations for Nu and Sh numbers which will generally be time dependent. The most obvious transient to be chosen for a vaporizing droplet is the one observed when an initially homogeneous droplet is thrown into a high-temperature environment. The physical picture may be sketched as follows.

- Especially at low droplet temperatures—which is initially the case—liquid Pr and Sc numbers are large so that the time scale for momentum diffusion is comparatively short and a spherical vortex (Hill's vortex) is established quickly.
- The turn-around time in the spherical vortex is short compared to characteristic times of heat and mass diffusion, so that properties along streamlines are approximately constant and heat and mass diffusion is normal to the streamlines, from the surface to the core. The effect of the vortex is thus to reduce the diffusional length scale L from surface to droplet core. The case of constant properties along streamlines is termed the Kronig–Brink [19] limit by Johns and Beckmann [20].
- For heat and mass transfer, we initially have a penetration problem. Liquid boundary layers are thin and growing, liquid Nu and Sh are large and decreasing.
- Eventually, the liquid boundary layers start to feel the symmetry boundary condition at the core, the temperature and concentration profiles become self-similar. This happens at times of about L^2/α and L^2/D for heat and species, respectively.

Johns and Beckmann [20] in 1966 were already aware of this self-similarity and based their mass transfer coefficients on the difference between surface and average liquid composition to obtain asymptotically constant Sherwood numbers.

Renksizbulut et al. [4] used the following correlations for liquid Nu and Sh numbers, in which the above physical picture is reflected

$$Nu_l = 22$$

$$Sh_l = 22 + \frac{5}{\sqrt{Fo}}\exp(-16\,Fo). \tag{13}$$

Here, $Fo = \bar{D}_l t/R^2$ and average liquid values are used for D, k and ρ. The interpretation of the constant Nusselt number is that temperature profiles become self-similar much faster than concentration profiles due to the large liquid Lewis number. Indeed $Le_l \gg 1$ especially at low liquid temperatures, which is initially the case.

For the present investigation we used Nusselt and Sherwood correlations from Renksizbulut et al., unless noted otherwise.

2.3. Estimation of properties

The following properties are needed for both liquid and gas phase: thermal equation of state (EOS); caloric EOS; dynamic viscosity; thermal conductivity; and 'effective' diffusion coefficient D_{im}, i.e. the diffusion coefficient of species i in mixture. Here, we make the assumption that diffusion can be calculated using D_{im} instead of solving the more rigorous diffusion equation based on binary diffusion coefficients D_{ij}. In addition, we need the latent heat and conditions for the VLE. If we want to calculate Weber and Ohnesorge numbers to test for droplet stability, we also need the surface tension.

Because data are not always available, especially at high pressures and for mixtures, property estimation methods are needed. Estimation methods have also the advantage that only a comparatively small number of characteristic constants is needed for each species and new species may be added to the database in little time. All the constants needed for the estimation methods in Table 2 can be found in Reid et al. [21].

For the estimation of above properties, it is simplest to make the ideal-gas assumption and to neglect the effect of pressure on liquid properties and transport coefficients. However, in modern gas turbines, pressures may exceed 30 bar while in modern diesel engines they may well rise above 120 bar. Critical pressures of heavy normal paraffins typically contained in diesel-fuel range from about 10–20 bar, which means that pressures may be (far) supercritical in these applications, and ideal-gas behavior cannot be expected.

Table 2
Property estimation methods

	Low-pressure PEM		High-pressure PEM	
	Liquid	Gas	Liquid	Gas
Thermal EOS	Watson method, simplified for low T, p [22]	Ideal-gas law	Peng–Robinson EOS	
Caloric EOS	Via latent heat and c_p of gas	Empirical third-order polynomial in T	Ideal-gas c_p and correction using Peng–Robinson EOS	
VLE	Raoult's law		Fuel species: equal chemical potentials (using Peng–Robinson EOS); ambient species: insolubility condition	
Latent heat	Latent heat of pure species; Pitzer accentric factor correlation		Peng–Robinson EOS	
Surface tension	Macleod–Sugden correlation		Macleod–Sugden correlation	
Dynamic viscosity	Pure species: empirical fits; mixture: molar average	Lucas method, simplified for low p and non-polar gases	Same as low-p method, but using high-p correction by Lucas	Lucas method, simplified for non-polar gases
Thermal conductivity	Sato–Riedel method with mixing rule by Li	Chung et al. method, simplified for low pressure, for non-polar and non-associating gases	Same as low-p method	Chung et al. method, simplified for non-polar, non-associating gases
'Effective' diffusion coefficient	Hayduk and Minhas method for n-paraffins; mixing rule by Perkins and Geankoplis	Binary diffusion coeff.: Fuller et al. method; 'effective' diffusion coeff.: CHEMKIN [23]	Same as low-p method, but using high-p viscosities	Same as low-p method, but using high-p correction by Takahashi

We decided to equip the zero-dimensional vaporization model with two different sets of PEM: (i) simplified methods based on ideal-gas behavior and neglecting the influence of high pressure; and (ii) general methods taking into account real-gas behavior and the effect of high pressure on various properties. The motivation for using two distinct PEM packages was to save computational time in applications that feature low pressures, since high-p PEM are comparatively expensive, especially in the case of mixtures.

Table 2 shows short descriptions of the various PEM. The upper half of the table contains thermodynamic equilibrium properties, the lower half molecular transport coefficients. Most of the methods can be found in [21] and are therefore not explicitly referenced.

As VLE condition for the low-p PEM we use Raoult's law, generalized for multiple species:

$$X_{gsi} = X_{lsi}\frac{p_{vi}}{p} \quad i = 1,\ldots,F.$$

In the high-p PEM, the estimation of thermodynamic equilibrium properties is mostly based on the Peng–Robinson EOS which has been widely used and represents well vapor–liquid equilibrium at high pressures [24]. For real gases and liquids at high pressures, the molar heat capacity C_p is calculated from the ideal-gas-mixture heat capacity C_p^0 and a residual heat capacity ΔC_p

$$C_p = C_p^0 + \Delta C_p$$

where

$$\Delta C_p = T\int_{\infty}^{V}\left(\frac{\partial^2 p}{\partial T^2}\right)_{V,X_i} dV - \frac{T(\partial p/\partial T)^2_{V,X_i}}{(\partial p/\partial V)_{T,X_i}} - R \tag{14}$$

and the integral and the derivatives in (14) can be calculated analytically for the Peng–Robinson EOS.

For VLE, the high-pressure method starts from the general requirement of equal chemical potentials or, equivalently, equal fugacities

$$f_{lsi} = f_{gsi} \tag{15}$$

in either phase for each species. Using the Peng–Robinson EOS, the fugacities can be expressed in terms of the independent variables p, T and X_i, as shown in [24].

Figure 1 compares VLE results of Raoult's law and Peng–Robinson EOS for the n-decane/nitrogen binary system. As can be seen, the Peng–Robinson EOS yields higher n-decane mass fractions in the gas phase, with differences increasing as pressure increases. Also, according to the Peng–Robinson EOS, with increasing pressure an increasing amount of nitrogen is dissolved in the liquid. For our model, however, we decided to neglect the solubility of any ambient (or non-fuel) species such as nitrogen in the liquid even when using high-p PEM. Our reasons for doing this are as follows: (i) we obtain a reduced number of equations and unknowns and thus a simplified model; (ii) even at diesel-engine pressures, during most of a droplet's lifetime, nitrogen mass fractions in the liquid at the surface remain below 10% (see e.g. [9]), an error which is small compared to the 50% difference in fuel mass fraction in the gas between Raoult's law and Peng–Robinson EOS at a reduced pressure of four (see Fig. 1); (iii) the situation in which liquid nitrogen mass fraction becomes biggest is when the surface closely approaches the critical state; in this case, however, liquid and gas densities approach each other so that the assumption of a quasi-steady gas boundary layer surrounding the droplet must be expected to fail and transient phenomena will limit the accuracy of the model.

The partial molar latent heats

$$L_i \equiv H_{gsi} - H_{lsi}$$

needed for the mass-flow-rate-averaged latent heat are expressed in terms of fugacities in the high-pressure method

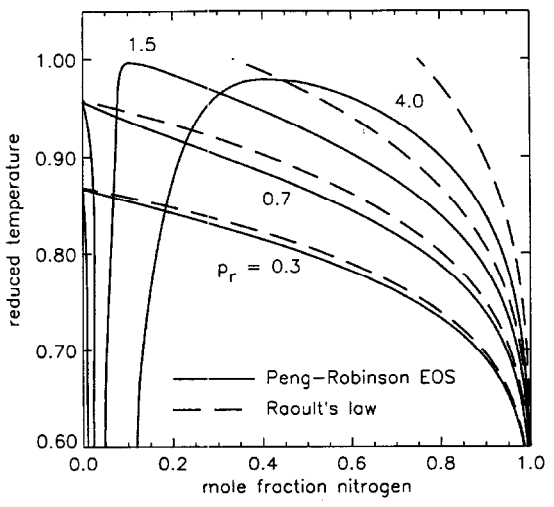

Fig. 1. Comparison of liquid (left curves) and gas (right curves) phase as a function of reduced temperature and pressure for the n-decane/nitrogen system.

$$L_i = RT^2 \left[\left(\frac{\partial \ln f_{lsi}}{\partial T} \right)_{p,X_i} - \left(\frac{\partial \ln f_{gsi}}{\partial T} \right)_{p,X_i} \right] \tag{16}$$

see e.g. Stephan and Mayinger [25]. In (16), we evaluate the temperature derivatives numerically.

For estimation of gas-phase transport coefficients, we simplified most methods for non-polar and non-associating compounds, since we are interested in the vaporization of diesel-fuel droplets, which are composed mostly of heavy non-polar hydrocarbons.

Heating to the Critical State. At sufficiently high ambient pressures and temperatures, a droplet may heat to the critical state [26]. We stop the integration as soon as the surface of the droplet has reached critical state, since with surface tension equal to zero, the droplet is subject to rapid disruption and diffusion.

In the low-p PEM, we assume that the surface has reached critical state as soon as the surface temperature has approached the critical temperature of the heaviest species to some ΔT, for which we choose a small, but finite value (e.g. 3K) to avoid numerical difficulties at the critical temperature.

For supercritical pressures, critical state is reached at temperatures lower than the critical one of the heaviest species. Therefore, a more general criterion is employed for the high-p PEM. As an indicator of how close the surface has approached critical state, we use the parameter

$$a \equiv \mathrm{d}L'/\mathrm{d}T_r \tag{17}$$

which is the derivative of the normalized latent heat $L' = L/L_R$ with respect to reduced temperature $T_r = T/T_{cH}$. Here, T_{cH} is the critical temperature of the heaviest fuel species and L_R is a reference latent heat at low temperatures which we set to $2.5 \cdot 10^5$ J/(kg K). Near the critical state, the latent heat sharply drops to zero, so that we use the criterion

critical state $\Leftrightarrow a \leqslant a_c$.

We set a_c to -20, but any value between about -10 and -50 works fine and gives similar results.

Special Treatment of Light Liquid Components. In a bicomponent droplet it may happen that the surface temperature as well as the average temperature exceed the critical temperature T_{cL} of the lighter component. In spite of the preferential vaporization of the lighter component, there may be some amount of this component left in the droplet when T_{cL} is reached. In this case, for the light component we linearly extrapolate the vapor pressure curve beyond the critical point to be able to still use Raoult's law for the low-p PEM; we assume the latent heat to be zero if $T \geqslant T_{cL}$ for the low-p PEM; and we (arbitrarily) limit T to 0.75 T_{cL} in liquid estimation methods which become singular at T_{cL}.

3. Numerical procedure

For a total of N species, F of which are fuel species, there is a vector $\mathbf{y}(t)$ of $F+4$ unknown droplet quantities

which must be integrated in time. Our choice of unknowns is

$$\mathbf{y}(t) = \{m, \bar{Y}_{l1}, \ldots, \bar{Y}_{l(F-1)}, \bar{T}_l, v_x, v_y, v_z\}.$$

In addition, we use a vector of unknown surface properties and flow rates at the surface of length $N+F+1$,

$$\mathbf{x}(t) = \{\dot{m}, \dot{Q}_g, T_s, Y_{ls1}, \ldots, Y_{ls(F-1)}\, Y_{gs1}, \ldots, Y_{gs(N-1)}\}.$$

For integration of $\mathbf{y}$, equations (1)–(4) are used, which may be written in short form

$$\frac{d\mathbf{y}}{dt} = \mathbf{f}(\mathbf{x}, \mathbf{y}, t). \tag{18}$$

For the additional unknowns $\mathbf{x}$, there are $N+F+1$ algebraic equations:

- F VLE conditions [equations (15) for $i = 1, \ldots, F$],
- N-1 species flow rates to match at the surface [equations (9)],
- one energy surface conditions [equation (10)] and
- one expression for $\dot{Q}_g$ [equation (6)].

The algebraic or constraint equations can be written as

$$\mathbf{0} = \mathbf{g}(\mathbf{x}, \mathbf{y}, t). \tag{19}$$

Equations (18) and (19) constitute a set of differential-algebraic equations.

For time integration, we use the classical fourth-order-accurate explicit Runge–Kutta scheme, while we iteratively solve the nonlinear system (19) at every Runge–Kutta substep. The solution of (19) is by far the most expensive part of the calculation, which is why we chose a high-order scheme in time, allowing for comparatively large time steps.

Initial-Guess Procedure. Solution of the nonlinear system (19) of constraint equations is by iteration, so that an initial guess is needed. During the time integration, the solution $\mathbf{x}$ of the previous time step or previous Runge–Kutta substep, respectively, is taken as the new initial guess for $\mathbf{x}$. At the beginning of the time integration, however, no previous solution of $\mathbf{x}$ is available. To find an initial solution for $\mathbf{x}$, we use the following algorithm:

(1) Assume the droplet to be 'well-stirred'. This leads to a simplified problem, for which an initial guess can be made: the liquid surface state is equal to the initial average liquid state; the gas composition can approximately be determined from Raoult's law and $\dot{m}$ and $\dot{Q}_g$ can be estimated from equations (6) and (8). Since the actual droplet is not 'well-stirred', the solver may fail to converge. If this happens

(2) Liquid Nusselt and Sherwood numbers are raised to make the problem for which the initial solution is sought more similar to the problem for which the initial guess is supposed to be good. After convergence is obtained, Nu_l and Sh_l are re-lowered step by step down to their original values. For each new (lower) values of Nu_l and Sh_l, the solution of the previous problem (with higher Nu_l and Sh_l) is taken as initial guess.

4. Model evaluation

In order to assess the accuracy and predictive capability of the zero-dimensional vaporization model, we compared results obtained with this model to experimental and numerical data found in the literature.

The first two comparisons presented are mainly a test on liquid Nusselt and Sherwood correlations. Abramzon and Sirignano [3] considered an n-decane droplet of initial diameter $D_0 = 50$ μm and initial velocity $V_0 = 15$ m s^{-1}, vaporizing in nitrogen at 10 bar and 1500 K. They used an extended model where heat transfer in the liquid was calculated solving a 2-D energy equation and taking Hill's vortex as the velocity field. In Figs. 2 and 3, tem-

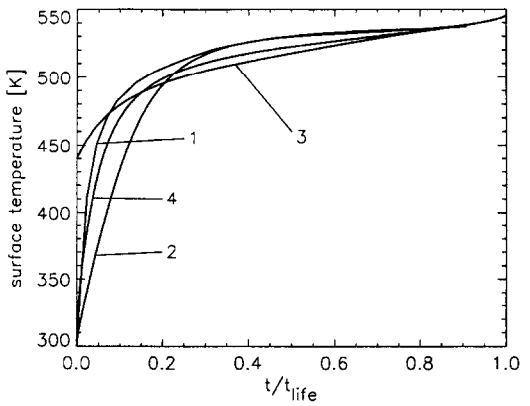

Fig. 2. Comparison with Abramzon and Sirignano: surface temperature. (1) Abramzon and Sirignano, extended model; (2) present model, well stirred droplet; (3) present model, $Nu_l = 22$; (4) present model, Nu_l made symmetric to Sh_l.

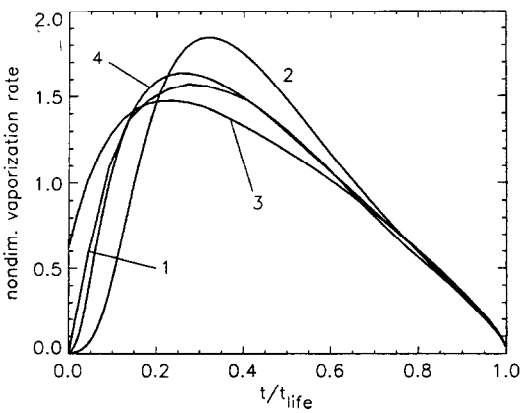

Fig. 3. Comparison with Abramzon and Sirignano: nondimensional vaporization rate. Cases: see Fig. 2.

poral evolution of droplet surface temperature and vaporization rate are shown as obtained by Abramzon and Sirignano and by the present model. Results of the present model were obtained with three different Nu_l correlations. As expected, in the well-stirred limit ($Nu_l \to \infty$), surface temperature and vaporization rate are initially too low. Using $Nu_l = 22$ results only in a slight improvement, with initially too high surface temperature and vaporization rate. It is interesting to note, however, that if Nu_l is made symmetric to Sh_l in equation (13) to account for the initial penetration of heat into the droplet, agreement in both temperature and vaporization rate is significantly improved.

Next, results of the present model are compared to measurement made by Randolph et al. [27] of droplets freely falling in a hot air stream at atmospheric pressure. These measurements are particularly relevant to us because bicomponent droplets were used of species typically found in diesel fuel. For different volatility differentials, i.e. for mixtures of n-$C_{16}H_{34}$/n-$C_{14}H_{30}$, n-$C_{16}H_{34}$/n-$C_{12}H_{26}$ and n-$C_{16}H_{34}$/n-$C_{10}H_{22}$, respectively, Randolph et al. measured droplet average composition vs. size. The data are shown in Fig. 4 along with the results of the zero-dimensional model. As can be seen, there is good agreement for the lowest and highest volatility differential, while the model gives a somewhat less pronounced sequential vaporization for the intermediate volatility differential.

From the two examples presented one gets the impression that the zero-dimensional vaporization model is able to account for droplet-internal transport with a sufficient degree of accuracy, even though only mass-averaged and surface properties are used.

In the next case, we compare wet-bulb temperatures (T_{WB}) as a function of ambient pressure and temperature, which is mainly a test of VLE condition and gas-phase properties. For a suspended n-heptane droplet, Savery and Borman [28] measured wet-bulb temperatures for pressures up to 100 atm. Their data are compared with results of the present model using low-p and high-p PEM in Fig. 5. As can be seen, the agreement is generally good for both PEM. The results of low-p and high-p PEM are quite close except for the very highest pressures and temperature, where the low-p PEM give too high values of T_{WB}, which is mainly because Raoult's law underestimates the fuel mass fraction in the gas (see Fig. 1).

The last test case we present is one that is inherently difficult for the model, but at the same time is of great practical relevance. Under ambient conditions typical of diesel engines, droplets may well heat to the critical state, i.e. to the point when the droplet surface becomes critical. Under these conditions, liquid and gas densities approach each other and the assumption of a QS boundary layer around the droplet must be expected to eventually fail. Nevertheless, zero-dimensional models are widely used (see e.g. [29]), and will continue to be used, under such conditions because of limitations in computer resources. It is therefore important to investigate the zero-dimensional model's behavior under conditions close to critical. One interesting question is under what ambient conditions the droplet approaches critical state. In the plane of reduced ambient pressure and temperature, it is possible to draw a hyperbola-type curve which we will call 'critical curve' (CC). For pressure and temperatures to the upper/right of the CC, droplets will reach critical state, while for pressures and temperature to the lower left, they will not. Using a detailed 1-D model (see Table

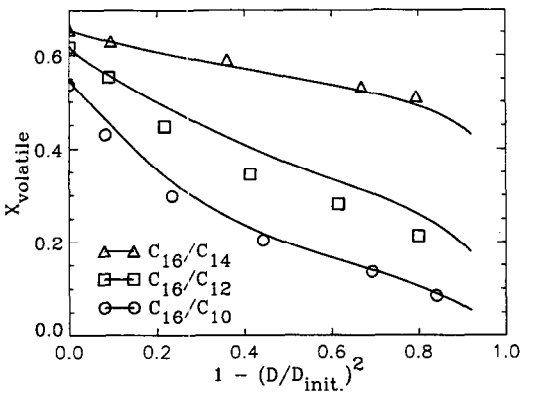

Fig. 4. Comparison with Randolph et al.: average mole fraction of volatile species as a function of droplet size. Symbols: measurements; lines: present model.

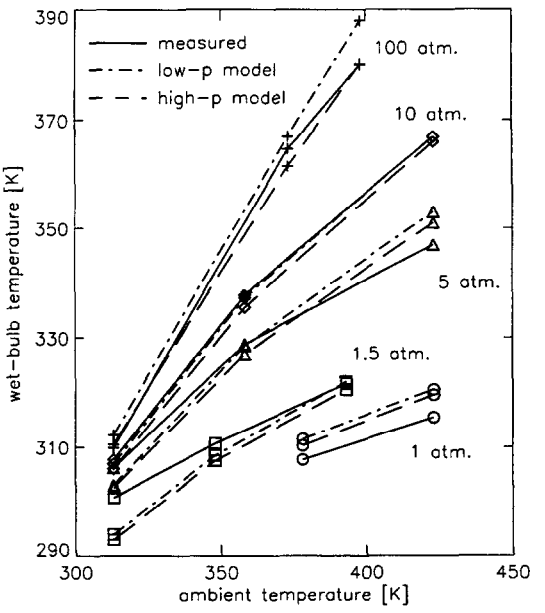

Fig. 5. Comparison with Savery and Borman: wet-bulb temperature as a function of ambient pressure and temperature.

1), Curtis and Farrell found the CC to be quite species independent for n-C_7H_{16}, n-C_8H_{18} and n-$C_{12}H_{26}$; this curve is shown as a dashed line in Fig. 6. Using the zero-dimensional model with high-p PEM, we obtained for n-C_7H_{16} a CC which is, although having qualitatively the right shape, located at too low pressures and temperatures. In other words, according to the model, droplets heat to the critical state too soon. Our way to remedy this discrepancy is to correct (to lower) Nu_g for near-critical conditions. From a theoretical point of view, our justification for this correction is that, as mentioned, the QS assumption must be expected to fail near the critical state; and that heat transfer cannot be expressed as in equation (6) if there is enthalpy diffusion, an effect which can easily be of importance. The correction factor C_{Nu} we use to multiply Nu_g is

$$C_{Nu} = 1 - \Delta C_{Nu}(1 - \mathrm{erf}((9+a)/2.5)$$

$$\Delta C_{Nu} = 0.52(1 - \exp(-0.011 \cdot 10^{-5} p))$$

where a as defined in equation (17) is a measure of how close critical state is approached and p is in Pa. Far from critical state, $C_{Nu} \to 1$. This expression for C_{Nu} gives good results for the CC for different normal paraffins and pressures up to 110 bar, as can be seen in Fig. 6.

Finally, we would like to make a note on the accuracy that may be obtained when predicting droplet lifetimes. We compared lifetimes from the present model with various sources of numerical and experimental data from the literature and found differences in the range of 10–15% not to be unusual for cases of high ambient temperature. We account these relatively high differences mainly to uncertainties in gas phase properties and to uncertainties in gas-phase correlations and gas reference state (to take into account effects of variable properties), while liquid-internal transport has a somewhat less pronounced effect on lifetime. Finally, one must not forget that expressions (5) to (8) do not allow cross effects between heat and mass transfer such as Soret and Dufour effect and enthalpy diffusion to be directly taken into account, setting fundamental limits to the accuracy of this simplified model.

5. Effects of property estimation methods

In what follows we will present results obtained with the zero-dimensional model for a droplet vaporizing under ambient conditions typical of a gas-turbine-combustor environment. We use the example to compare in some detail results of low- and high-p PEM, to get a feeling for the magnitude of differences and for the range of applicability of the (cheaper) low-p PEM.

Parameters for the gas-turbine (GT) droplet are summarized as follows: pressure $p = 20$ bar, ambient temperature $T_\infty = 800$ K, initial droplet temperature $T_l = 400$ K. Initial droplet composition: n-$C_{10}H_{22}$ and n-$C_{16}H_{34}$ with $Y_{lC10} = 0.4$; $Y_{lC16} = 0.6$, ambient gas N_2, initial gas-droplet relative velocity $V = 25$ m s^{-1}, initial droplet mass $m = 2.56$e-12 kg. Initial radius: low-p PEM $R = 9.64$ μm, high-p PEM $R = 10$ μm. No radiation; zero gravity.

Figures 7 to 10 show the vaporization history of the droplet comparing low-p and high-p PEM. Figure 7 shows droplet mass, diameter squared, relative velocity, and average and surface temperature versus time. Temperatures continuously rise and no wet-bulb state is attained. Initial surface temperature is about 50 K above average temperature, facilitating early vaporization (see the initially quite high vaporization rate of n-decane in Fig. 10).

The low-p PEM give a droplet lifetime which is about 23% longer than that obtained with the high-p PEM. About half this difference may be accounted to different VLE and latent-heat estimation methods: if high-p PEM are used, but VLE and latent heat are calculated as in the

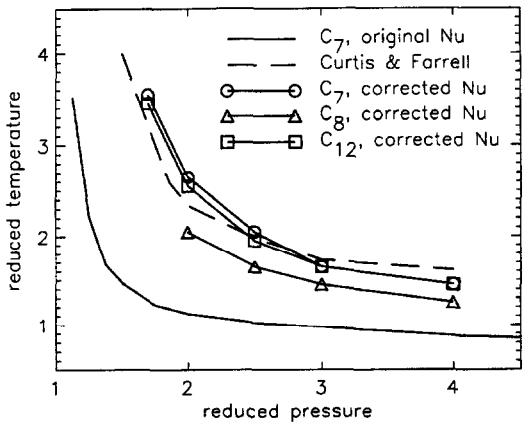

Fig. 6. Comparison with Curtis and Farrell: critical curve indicating ambient conditions for which droplets reach critical state.

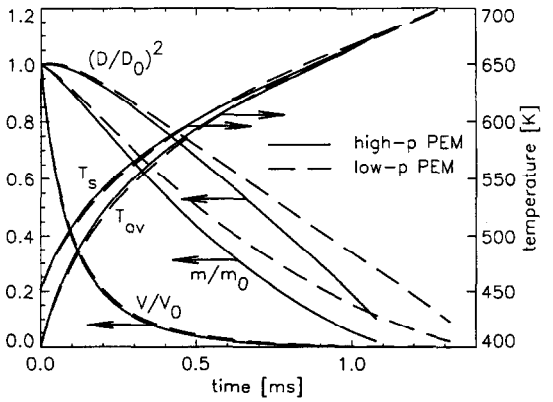

Fig. 7. Typical GT droplet: diameter squared D^2, mass m and relative velocity V, normalized by initial values (index '0'); droplet average temperature T_{av} and surface temperature T_s.

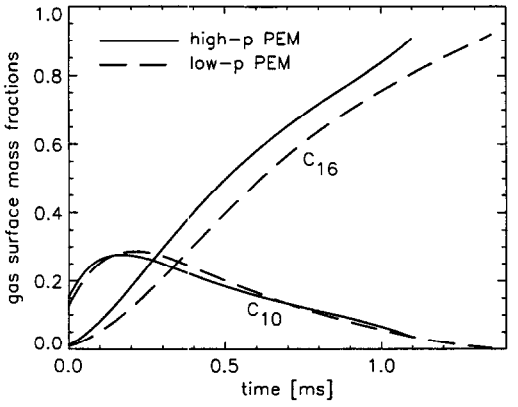

Fig. 8. Typical GT droplet: composition of gas at surface: mass fractions of *n*-decane and *n*-hexadecane.

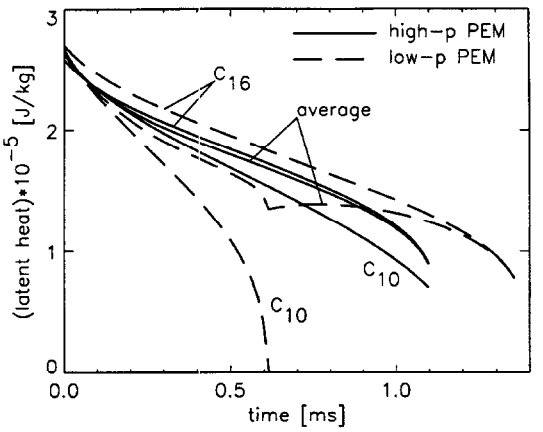

Fig. 9. Typical GT droplet: latent heats of *n*-decane and *n*-hexadecane and mass-flow-rate-averaged latent heat.

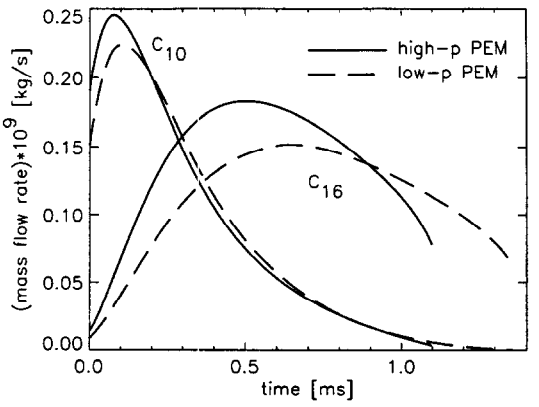

Fig. 10. Typical GT droplet: mass flow rates through droplet surface of *n*-decane and *n*-hexadecane.

low-*p* PEM, the lifetime is too long by about 11%. This influence of PEM on lifetime may be compared to the influence of other factors. Using the 'classical' correlations for Nu_g and Sh_g [equations (11) and (12)] together with the 1/3-rule results in about 10% shorter lifetimes, while Abramzon and Sirignano's correlation give a lifetime lying between these values. Varying the gas reference state from pure surface to pure ambient results in lifetimes different by about 6%. It is important to note, however, that the influence of the reference state increases with increasing ambient temperature T_∞. For $T_\infty = 1500$ K lifetimes may easily differ by as much as 30–40%, with the pure ambient reference state giving the shortest lifetimes. Finally, using the well-stirred droplet model gives a lifetime about 4% shorter.

Figure 8 shows the composition of the gas at the droplet surface vs. time. For the heavier component (*n*-hexadecane), as suggested by Fig. 1, gas-phase mass fractions are underestimated by Raoult's law, while for the lighter component *n*-decane, differences are smaller and of changing sign.

In Fig. 9, latent heats of *n*-decane and *n*-hexadecane are shown together with the mass-flow-rate-averaged latent heat. The latent heat of *n*-hexadecane is overestimated by the low-*p* PEM, while the latent heat of *n*-decane is severely underestimated and hits zero as soon as the surface temperature reaches the critical temperature of *n*-decane (as discussed in Section 2.3). This causes an ugly cusp in the averaged latent heat of the low-*p* PEM. With the underestimated latent heat of *n*-decane dominating, the average latent of the low-*p* PEM is lower than the one of the high-*p* PEM, especially near the critical temperature of *n*-decane.

Figure 10 shows the vaporization rates of *n*-decane and *n*-hexadecane. The curves of $\dot{m}_{C10}$ and $\dot{m}_{C16}$ reflect the expected preferential vaporization of *n*-decane, with $\dot{m}_{C10}$ peaking earlier than $\dot{m}_{C16}$. With the low-*p* PEM, *n*-hexadecane vaporizes clearly slower than with the high-*p* PEM, which is because of the too low *n*-hexadecane mass fraction in the gas at the surface (Fig. 8), which constitutes the driving potential for *n*-hexadecane mass transfer. On the other hand, *n*-decane vaporizes at about the same rate with both low-*p* PEM and high-*p* PEM.

The differences between low- and high-*p* PEM may be summarized as follows:

- For the heavy component (*n*-hexadecane), gas surface mass fraction is underpredicted by Raoult's law as suggested by Fig. 1. The reduced driving potential for the heavy component leads to a slower vaporization of the latter with the low-*p* PEM, causing the longer droplet lifetime.
- Since the lighter component (*n*-decane) vaporizes almost equally fast with either set of PEM, the volatility differential between *n*-decane and *n*-hexadecane seemingly increases with the low-*p* PEM.

6. Conclusions

Zero-dimensional droplet vaporization models are attractive for spray simulation because of their relatively low demand on storage and CPU time. The accuracy of the zero-dimensional model depends on liquid and gas Nusselt and Sherwood correlations, on the reference-state scheme and on PEM. If appropriate Nu_l and Sh_l numbers are used, transient heating and multicomponent vaporization can be predicted with sufficient accuracy. For elevated pressures as encountered in gas-turbine combustors and diesel engines, high-p PEM should be used. For near-critical conditions as may occur in diesel engines, the quasi-steady assumption in the gas phase becomes invalid since liquid and gas densities approach each other. With appropriate corrections to Nu_g and/or Sh_g it is, however, possible to predict heating to the critical state under the correct ambient conditions.

We would like to mention that there is a need for more data on single-droplet vaporization under well characterized conditions, to be able to further evaluate correlations for Nusselt and Sherwood numbers and drag coefficient. Data are particularly needed at high pressures, for multicomponent droplets and with forced convection.

Acknowledgements

Financial support for this work has been provided by the Swiss Federal Office of Energy (BEW) in the frame of a collaboration with Asea Brown Boveri and the Paul Scherrer Institute. We would like to thank Dr F. Tanner at our institute and Professor A. Tomboulides at Boston University for fruitful discussions.

References

[1] Shirolkar JS, Coimbra CFM, Queiroz McQuay M. Fundamental aspects of modeling turbulent particle dispersion in dilute flows. Progress in Energy and Combustion Science 1996;22:363–99.

[2] Ayoub NS, Reitz RD. Multidimensional Computation of Multicomponent Spray Vaporization and Combustion. Report 950285, SAE, 1995.

[3] Abramzon B, Sirignano WA. Droplet vaporization model for spray combustion calculations. International Journal of Heat and Mass Transfer 1989; 32:1605–18.

[4] Renksizbulut M, Bussmann M, Li X. A droplet vaporization model for spray calculations. Particle–Particle System Characterization 1992;9:59–65.

[5] Matlosz RL, Leipziger S, and Torda TP. Investigation of liquid drop evaporation in a high-temperature and high-pressure environment. Journal of Heat and Mass Transfer 1972;15:831–52.

[6] Curtis EW, Farrell PV. A numerical study of high-pressure droplet vaporization. Combustion and Flame 1992;90:85–102.

[7] Hsieh KC, Shuen J.-S, Yang V. Droplet vaporization in high-pressure environments, I: near critical conditions. Combustion Science and Technology 1991;76:111–32.

[8] Stengele J, Bauer H.-J, Wittig S. Numerical Study of Bicomponent Droplet Vaporization in a High Pressure Environment. 96-GT-442, ASME, 1996.

[9] Jia H, Gogos G. High pressure droplet vaporization; effects of liquid-phase gas solubility. International Journal of Heat and Mass Transfer 1993;36(18):4419–31.

[10] Megaridis CM. Liquid-phase variable property effects in multicomponent droplet convective evaporation. Combustion Science and Technology 1993;92:291–311.

[11] Varnavas C, Assanis D. An improved model for predicting evaporation of high-pressure engine sprays. Proceedings of the Sixth International ICLASS Conference on Liquid Atomization and Sprays. Rouen, France, 1994, pp. 97–104.

[12] Jin JD and Borman GL. A Model for Multicomponent Droplet Vaporization at High Ambient Pressures. Report 850264, SAE. 1985.

[13] Haywood RJ, Nafziger R, Renksizbulut M. A detailed examination of gas and liquid phase transient processes in convective droplet evaporation. Journal of Heat Transfer 1989;111:495–502.

[14] Kuo KK, Principles of Combustion, 1st ed. New York: Wiley, 1989, p. 374.

[15] Ranz WE, Marshall WR. Evaporation from drops (parts I and II). Chemical Engineering Progress 1952;48:141–6, 173–80.

[16] Bird, RB, Stewart WE, Lightfoot EN. Transport Phenomena, 1st ed. New York: Wiley, 1960, p. 658.

[17] Renksizbulut M, Yuen MC. Experimental study of droplet evaporation in a high-temperature air stream. Journal of Heat Transfer 1983;105:384–8.

[18] Renksizbulut M, Nafziger R, Li X. A mass transfer correlation for droplet evaporation in high-temperature flows. Chemical Engineering Science 1991;46:2351–8.

[19] Kronig R, Brink JC. On the theory of extraction from falling droplets. Applied Scientific Research 1950;A-2:142–54.

[20] Johns LE, Beckmann RB. Mechanisms of dispersed-phase mass transfer in viscous, single-drop extraction systems. AIChE Journal 1966;12:12–6.

[21] Reid RC, Prausnitz JM, Poling BE. The Properties of Liquids and Gases, 4th ed. New York: McGraw-Hill, 1987.

[22] VDI-Gesellschaft Verfahrenstechnik und Chemieingenieurwesen (GVC), Verein Deutscher Ingenieure. VDI Heat Atlas, 6th ed. Verlag: VDI, 1993.

[23] Kee RJ, Dixon-Lewis G, Warnatz J, Coltrin ME, Miller JA. A Fortran Computer Code Package for the Evaluation of Gas-Phase Multicomponent Transport Properties. SAND86-8246, CA, U.S.A.: Sandia National Laboratories, 1993.

[24] Ohe S. Vapor–Liquid Equilibrium at High Pressure, 1st ed. New York: Elsevier, 1990.

[25] Stephan K, Mayinger F. Thermodynamik: Band 2, Mehrstoffsysteme und Chemische Reaktionen, 13th ed. New York: Springer, 1992.

[26] Givler SD, Abraham J. Supercritical droplet vaporization and combustion studies. Progress in Energy and Combustion Science 1996;22:1–28.

[27] Randolph AL, Makino A, Law CK. Liquid-phase diffusional resistance in multicomponent droplet gasification. Twenty-first Symposium (International) on Combustion. The Combustion Institute, 1986, pp. 601–8.

[28] Savery W, Borman GL. Experiments on droplet vaporization at supercritical pressures, AIAA Eighth Aerospace Sciences Meeting, 1970, Paper No. 70-6.

[29] Amsden AA, O'Rourke PJ, Butler TD. KIVA-II: A Computer Program for Chemically Reactive Flows with Sprays, Los Alamos, New Mexico, U.S.A.: Los Alamos, 1989.